Lab on a Chip

Cite this: *Lab Chip*, 2011, **11**, 1022

www.rsc.org/loc

PAPER

The separation of immiscible liquid slugs within plastic microchannels using a metallic hydrophilic sidestream

Frederik Scheiff,*[a] Matthias Mendorf,[a] David Agar,[a] Nuno Reis[b] and Malcolm Mackley[b]

Received 24th September 2010, Accepted 7th January 2011
DOI: 10.1039/c0lc00442a

This paper describes experiments and related modelling on a new method for separating aqueous phase slugs from the surrounding organic matrix phase in segmented two phase flow in a plastic microcapillary film (MCF). Kerosene or paraffin oil was metered through a plastic capillary of 630 microns diameter and aqueous phase slugs were generated within the capillary by the continuous sidestream injection of water. It was found that the resulting aqueous phase slugs formed in the MCF could be subsequently easily separated from the organic phase by piercing the downstream sidewall of the plastic capillary with a hydrophilic metal hypodermic needle to draw off an aqueous sidestream. Optical scrutiny of the phase separation process indicated that two distinct disengagement mechanisms are involved, in which the metal needle tip either remains submerged in the aqueous phase or becomes periodically exposed to the organic phase at certain stages of the segregation process. The separation efficiency, *i.e.* the degree of residual phase cross-contamination, was determined as a function of both the sidestream needle angle and the depth of needle penetration into the capillary for a given flow rate and phase ratio. It was established that the separation efficiency was very sensitive to the downstream pressure balance between the organic mainstream flow in the plastic capillary and the aqueous sidestream flow through the needle. A mathematical model for the pressure balance conditions was developed by making certain simplifying assumptions and taking the Laplace interfacial pressure into account. The model predictions agreed surprisingly well with the experimental findings, thus providing circumstantial evidence for the validity of the insights into the phase separation mechanism.

1. Introduction

The separation of liquid drops or slugs from a second immiscible liquid at both the macro- and microscale is a subject of considerable importance in chemical engineering. Gravitational or centrifugal separation based on density differences is often adopted at as a pragmatic and effective technique for industrial liquid–liquid decantation,[1] and in hydrocyclones for instance.[2,3] As a consequence of the continuing interest in the potential applications of microreactors and microprocessing in the chemical and biochemical industries, multiphase microfluidics is attracting increasing attention. It has also been gradually appreciated that organic/aqueous phase separation can be carried out very effectively on the microscale by exploiting wettability differences between the liquids on hydrophilic or hydrophobic surfaces. This paper brings together the elements of microcapillary slug flow and surface wettability discrimination to describe a new micro-mixer-settler arrangement specially tailored for microchannels.

Rapid phase separation, especially for fast biphasic reaction systems, can be crucial for enhancing yields, as in the case of an unwanted consecutive reaction of a product, and for otherwise eliminating unwanted stochastic factors and providing well-defined reaction conditions. Density-based processes are less suitable, or, in the case of gravitational separation, entirely inappropriate for small scale microfluidic devices in which surface forces often dominate.

For example, the resolution of fine dispersions or emulsions with droplet sizes down to 10 μm can be accomplished using microstructured separation nozzles,[4,5] in which the driving force for phase disengagement is the lift force induced by the shear stress on the surface of the dispersed phase. Phase separation can be achieved for liquids of similar densities without turbulence or high pressure drops.

For separating fine droplet suspensions, membranes are also a popular option,[6–8] which utilise the Laplace pressure inside the suspended phase to hinder access of the dispersed phase into the membrane. In some cases, small parallel microchannels in the range of 100–200 μm have been used instead of membranes to exploit capillary forces for phase separation purposes.[9,10]

[a]*Department of Biochemical and Chemical Engineering, TU University of Dortmund, Germany. E-mail: David.Agar@bci.tu-dortmund.de; Fax: +49 2317552698; Tel: +49 2317552799*
[b]*Department of Chemical Engineering and Biotechnology, University of Cambridge, UK. E-mail: mrm5@cam.ac.uk; Fax: +44 (0)1223 334796; Tel: +44 (0)1223 334784*

Wettability differences between the immiscible liquids can be used to enhance membrane separation processes.[7] A review of the literature reveals that the phase separation of gas–liquid phases is usually much easier, due to the higher interfacial surface tensions than in liquid–liquid systems, provided the pressure drop characteristics of the gaseous phase can be controlled so as to avoid a gas breakthrough.[8,11,12]

Exploiting the preferential surface wettability behaviour of liquids without the pressure drops arising in membranes appears to be a particularly promising approach for the liquid–liquid phase separation and the underlying principle has already been demonstrated experimentally by combining hydrophilic and hydrophobic regions within channels, to encourage immiscible liquids to separate.[13,14] Kashid and co-workers[15] described the very effective phase separation performance achieved using a simple PTFE Y-splitter unit, with a steel needle inserted as a liner into one of the two outlet lines. With this arrangement, it proved easy to obtain at least one pure phase and an only minor contamination of less than 5%, if any, in the other phase over a wide range of flow rates. Furthermore, this concept has been extended to multiple parallelised channels by Mendorf *et al.*,[16] who identified the pressure drop characteristic of the downstream equipment following the multichannel phase separator[16] as the most important factor determining the phase separation efficiency.

The phase separation experiments that are described in this paper were carried out in the recently devised plastic microcapillary films (MCFs).[17,18] MCFs are extruded plastic films that contain "*n*" parallel microchannels of predetermined diameter in the range 10 to 1000 microns, ideally 40 to 650 microns. The value of *n* depends on the extrusion die used and currently lies between 10 and 19 channels. The key features of the MCF of relevance to this paper are:

- the selected capillary diameter of 630 microns in a hydrophobic, high density polyethylene MCF film.
- the ability to introduce a metal hypodermic needle through the capillary wall without leakage.
- the ability to optically monitor the microscopic flow characteristics within the capillary through the flat MCF walls *via* two optically planar surfaces.

2. Experimental

2.1 Experimental setup

All microcapillary films (MCFs) used in this paper were prepared from a polyolefin plastomer resin (DOW Affinity®) using an in-house extrusion line. Nineteen capillaries with mean hydraulic diameters of 630 μm and diameter deviations of 5% in each capillary were embedded in films of 246 mm total length. In the experiments described in this paper, only one of the 19 microchannels was in fact used, although the principle can be easily extended for using multiple parallel channels.

The MCF material allowed observation of the liquid–liquid flow structure and the elasticity of the polymer guaranteed an adequate sealing when needles were inserted through the MCF capillary wall.

The separation of immiscible liquid slugs was investigated using deionised water as the slug-forming phase in the hydrophobic MCF capillary. Either kerosene (reagent grade, Sigma-Aldrich, Dorset, UK) or a higher viscosity mineral oil (BioReagent, Sigma-Aldrich, Dorset, UK) was used as the continuous organic flow medium. The similar interfacial tensions, γ_{i-j} of these two organic liquids with respect to water, together with their appreciable viscosity differences (μ_o) enabled the investigation of liquid–liquid separation for two distinct γ/μ ratios. Both γ and μ were determined experimentally and the resulting parameters are summarised in Table 1.

An in-house rheometer, a Piezo Axial Vibrator (PAV, University Cambridge),[19] was used to measure the viscosity of kerosene and mineral oil at 20.5 °C with an estimated error of 1%. Surface and interfacial tensions were determined by the capillary-rise method in an MCF at 20 °C. These values lie in the typical range for non-polar organic liquids. Errors in the values of surface-, interfacial tensions and contact angles were 13, 28 and 5%, respectively. The apparatus used for the phase separation experiments is shown schematically in Fig. 1.

The aqueous slug flow structure was generated in the MCF by a T-junction assembly using a hypodermic steel needle (BD Microlance™ 3, S 304). Two syringe pumps (Fresenius Injectomat S, Vickers Medical TREONIC IP5) were used to supply the aqueous and organic phase liquids. The continuous organic phase was metered into a 630 micron ID MCF capillary (d_M) through a 1.07 mm ID needle. A second needle was inserted at a given angle, Φ, into the MCF capillary and in the plane of the MCF film to a position where the needle tip just penetrated into the capillary. The slug-forming water phase was injected at right angles through this flat-tipped 0.82 mm needle. It was found that the exact degree of needle penetration in the capillary, ξ, and angle of the needle relative to the capillary wall, Φ, had only a marginal influence on the slug flow structure; this is shown below in this paper.

The phase separation section was assembled 150 mm downstream from the point of slug generation. For the separation of aqueous phase from the organic phase, a hydrophilic sidestream branch was fabricated by inserting a flat-tipped, hypodermic steel needle of 0.82 or 0.51 mm ID into the MCF capillary and connecting 1 mm ID silicon tubing to the needle stem. The capillary exit line, referred to as the mainstream outlet, was assembled by coupling the MCF outlet with 0.5 mm ID FEP

Table 1 Physical properties of liquids

Fluid	Density, ρ_i/ kg m^{-3}	Viscosity, μ_i/ N s m^{-2}	Surface tension, $\gamma_{i\text{-MCF}}$/N m^{-1}	Interfacial tension with water, γ_{i-j}/N m^{-1}	Contact angle, Θ_{i-j}/°
Water	998	0.0010	0.0212	—	—
Kerosene	787	0.0018	0.0397	0.0289	23.1
Mineral oil	840	0.0270	0.0386	0.0389	21.6

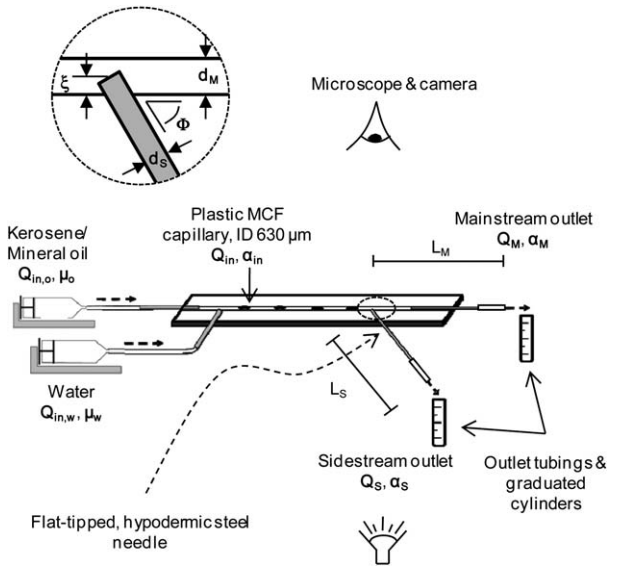

Fig. 1 Schematic of the experimental phase separation apparatus, showing both upstream injection and downstream phase separation setup and main separation parameters.

tubing (Upchurch Scientific, Oak Harbor, US) of various lengths using a 1.07 mm needle. The two outlets were fixed at the same height, thus equalising the hydrostatic pressures to within ±10 mm.

The separation efficiency was determined by collecting the homogeneous or biphasic outlet flows from both the sidestream and mainstream outlets in 5 mL graduated cylinders. Gravitational separation of the outlet material then enabled determination of the corresponding aqueous and organic liquid volumetric flow rates in the main- and sidestream outlets (Q_M and Q_S), as well as the volumetric fractions of water (α_S) in the sidestream and of the organic phase (α_M) in the mainstream, with a precision of better than 0.1 mL and 5%, respectively.

The flat shape and transparent nature of the MCF permitted fine adjustment of the needle position and microscopic optical monitoring of the separation process. A microscope with fivefold magnification (OLYMPUS BX 60) and a CCD camera (PROSILICA EC 1380C) were used for capturing 20 Hz snapshot sequences of the separation process.

The important geometrical parameters and process conditions are also represented in Fig. 1. The sidestream angle Φ and the degree of needle penetration ξ (*i.e.* the extent of the needle protruding into the MCF capillary), combined with the length L_S and internal diameter d_S of the sidestream branch, characterised the separator design. Due to their impact on the outlet pressure drops, the length and internal diameter of the mainstream outlet (L_M and d_M) also needed to be taken into consideration. According to the prevailing process conditions, inlet flow rates ($Q_{in,o}$, $Q_{in,w}$) and the properties of both phases dictate both the total flow rate Q_{in} and the aqueous fraction α_{in} of the slug flow in the MCF capillary.

Constant flow rates of 10 mL h^{-1} for each phase and an inlet aqueous fraction of α_{in} of 0.5 were employed in all experiments. These conditions led to a mean aqueous slug length of 2159 µm with a deviation of 12% in kerosene and 1265 µm with a 15% spread in mineral oil. All experiments were conducted at ambient temperature.

2.2 Influence of geometrical and physical parameters

The impact of fluid properties and junction point geometry on the separation process was analysed by characterising the separation efficiency as a function of:

- Fluid properties (kerosene/mineral oil–water)
- Internal diameter of sidestream needle, d_S (0.82 or 0.51 mm)
- Angle sidestream needle, Φ (30/50/70/90°)
- Degree of penetration of the needle in the capillary, ξ, with 3 scenarios tested: (a) $\xi < 30\%$ of d_M; (b) $\xi = 50\%$ of d_M; (c) $\xi > 70\%$ of d_M)

These parameters were varied systematically, using a matrix structured protocol of 48 experiments. Outlet lengths (L_M and L_S) and internal diameters (d_M and d_S) remained unchanged, in order to avoid pressure drop induced perturbations in the experiments.

Each measurement involved a precise installation of the sidestream branch with the geometrical parameters desired. These were checked with the optical measuring equipment and the open source image analysis tool ImageJ (NIH, USA).

After steady-state was established, the separation efficiency was measured as outlined above over a time interval of approximately 10 minutes. Additionally, a snapshot sequence of the separation process was recorded for each experiment.

2.3 Pressure balance

Separation efficiency was found to be particularly sensitive to the balance of pressure drops between the main- and sidestream outlets. This balance (and thus the separation performance) could be maintained and manipulated by altering the outlet geometries. Studies covering a range of mainstream outlet lengths L_M, while keeping the other parameters constant, were carried out for this purpose.

A suitable geometrical arrangement at the separation point was identified from the results of the sensitivity analysis conducted (0.51 mm ID flat-tipped sidestream needle, sidestream angles Φ of 88°, $\xi = 0.5\ d_M$ and a 175 mm long, 1 mm ID silicon sidestream tubing) and this experimental design was then used to observe the influence of the mainstream outlet length for:

- kerosene–water: 10 different lengths, ranging from 50 to 1650 mm and
- mineral oil–water: 8 different lengths, ranging from 5 to 290 mm.

In modelling terms, calculating the frictional pressure drops of liquid–liquid flow in the microcapillaries was based on the measured variables Q_i and α_i, and a modified Hagen–Poiseuille's relationship,[20] given in eqn (1), assuming fully developed heterogeneous, laminar flow with experimentally determined parameters for the two phase slug flow:

$$\Delta p_{H,i} = k_i'\left[\mu_o(1-\alpha_i) + \mu_w\alpha_i\right]Q_i \quad \text{with } k_i' = \frac{128L_1}{\pi d_1^4} \qquad (1)$$

where Q_i and α_i represent the flow rate and fluid fraction in the stream *i*. k_i' is the viscosity-independent pressure drop coefficient of stream *i* determined experimentally as follows. First, the pressure drop in the flowing outlet stream was measured using the static liquid height technique connected to the second outlet for the homogeneous flow of water at two different flow rates (10 mL

h^{-1} and 20 mL h^{-1}). Second, the coefficient k_i' was calculated from the resulting experimental data. Typically, the k_i' values obtained for the two outlet streams were within 5% variation.

After establishing the pressure drop coefficient with this technique for the sidestream, k_S', the protocol of each experiment involved two steps: (a) the coefficient k_M' was measured for a specific mainstream outlet configuration; (b) the pressure gauge at the sidestream outlet was removed and both outlets were flushed with water, before the separation experiment was conducted.

3. Experimental observations and results

3.1 Visualisation of slug separation

Optical inspection of the downstream junction of the plastic microcapillary and the metal sidestream needle enabled useful insight to be obtained into the separation process. Fig. 2 shows a time sequence of photographs taken at the downstream junction for "optimal" separation conditions. Flow was from left to right and the sidestream metallic hypodermic needle is shown as black. In Fig. 2a, a water slug approaches the needle. In Fig. 2c, the slug is above the needle and flowing into it. In Fig. 2d, a further slug has arrived at the needle. The main downstream capillary channel is essentially free of water at all times. In order to achieve these conditions, it was necessary to establish a correct "pressure balance" for the main- and sidestream sections, through a process described in further detail in section 4.

In general, two separation mechanisms were identified, examples of which are illustrated in Fig. 3. In mechanism A, observed for kerosene–water slug flow, the tip of the hypodermic needle remains covered by an aqueous layer throughout the process as portrayed photographically and schematically in Fig. 3a. Fig. 3b, observed for mineral oil–water slug flow, depicts mechanism B, in which the needle becomes exposed to the organic phase during part of the disengagement process. In this case, there is a period when the organic phase can flow down the hypodermic needle and separation efficiency is reduced.

3.2 Effect of sidestream needle angle (Φ) and degree of needle penetration (ξ)

Both the angle Φ (tested from 30 to 90 degrees) and degree of needle penetration ξ (tested for 30%, 50% and 70% of d_M) of the sidestream hypodermic needle were found to have a marginal effect on the separation efficiency. For example, in a given set of downstream conditions (sidestream tubing length of 196 mm and 202 mm for 0.82 mm and 0.51 mm ID hypodermic needles; mainstream outlet comprising MCF capillary, a 1.07 mm needle and a 30 mm long tubing; ξ at 50% of d_M), it was found that a value of Φ lower than 70 degrees resulted in significant sidestream contamination, whilst a value of $\Phi = 90$ degrees resulted in a volumetric water composition of 100% and 20% for the sidestream (α_S) and mainstream (α_M), respectively (results not shown). Therefore, the greatest value of $\Phi = 90°$ was selected for the detailed pressure balance studies. A second set of experiments for different degrees of penetration of the hypodermic needle into the plastic microcapillary channel had shown a relatively little effect on the water content of both the main- and sidestreams (results not shown), and the following pressure balance experiments were thus carried out with a 50% degree of needle penetration.

3.3 Influence of downstream pressure balance

The downstream pressure balance influenced the relative flow rates in the main- and sidestream capillaries as well as the water content in each stream. The measurement of the volumetric flow rates for both the main- and sidestreams, together with knowledge of the separation efficiency, in terms of volumetric aqueous fraction in the mainstream (α_M) and sidestream (α_S), made possible to use eqn (1) combined with the respective pressure drop coefficients k_i' to calculate the pressure drops for both the main- and sidestream lines. The length of the side- or mainstream lines could then be adjusted to give a precise "equilibrium set-point" for the two pressure drops. That "equilibrium set-point" occurs at an effective outlet length ratio, $L_M/L_S = 1$ when the internal diameter for the main- and sidestreams and viscosity of two liquids are identical. By varying L_M/L_S below or above the "equilibrium set-point" value, the effect of pressure drop divergence can be ascertained.

Fig. 4 shows the effect of L_M/L_S on separation efficiency, volumetric flow rate and pressure drop, respectively, for kerosene–water separation. In Fig. 4a it can be seen that the separation is most efficient for both the main- (organic) and sidestreams (aqueous) when L_M/L_S is in the range ~1 to 2. For a length ratio of L_M/L_S < ~1, the efficiency of separation of

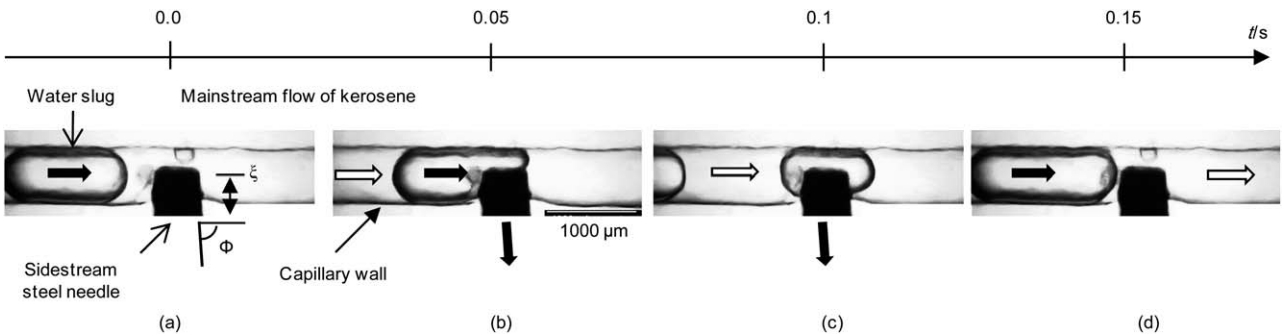

Fig. 2 Visualisation of water–kerosene slug separation in a MCF capillary. Flow is from left to right and the sidestream metal hypodermic needle is seen as black. A water slug approaches the needle in (a), and captured by the needle in (b). In (c) the remaining volume fraction of the slug is above the needle and will flow into the needle. In (d) a second slug approaches the needle. The main channel downstream the needle is essentially free of water at all times.

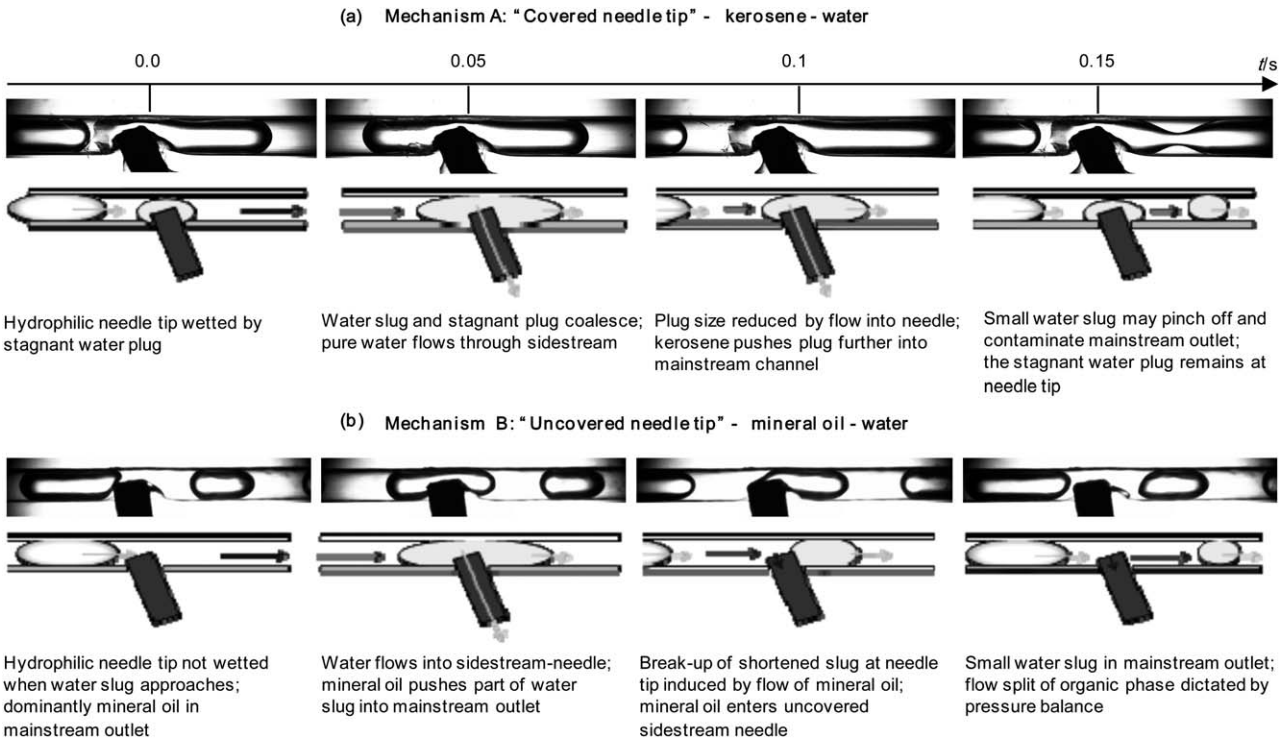

Fig. 3 Microscopic images and schematics of slug separation mechanisms A and B for the kerosene–water and mineral oil–water system, respectively.

water from the mainstream decreases and for a length ratio $L_M/L_S > \sim 2$ the volumetric composition of water in the aqueous sidestream deteriorates. Fig. 4b shows how the L_M/L_S length ratio influences the total flow distribution between the two outlet streams, Q_S/Q_M. When the L_M/L_S is between 1 and 2, equal volumetric flow rates of aqueous and organic phases flow in the respective side- and mainstreams, matching the upstream input flow rates in both cases. This is closely related with the pressure drop difference between the two outlet stream (Fig. 4c).

A similar effect of L_M/L_S on the separation of water from mineral oil (with a higher viscosity than kerosene) was also observed (results not shown). However, in this case the separation efficiency was greatly diminished and larger length ratios were required for reasonable segregation. In contrast to the results shown in Fig. 4 for kerosene–water, aqueous impurity levels in the mineral oil mainstream were relatively high, with the best separation conditions yielding 30% v/v of water in the mainstream.

4. Modelling of pressure balance and separation efficiency

4.1 Development of the pressure balance model

The experimental results reported in this paper showed that the separation of an aqueous slug dispersed in an organic phase depends on the hydrophilic/hydrophobic nature of the region of separation together with a pressure balance at the branch point. The additional Laplace pressure within the hydrophilic sidestream capillary associated with surface tension also plays a decisive role in the general efficiency of the aqueous–organic phase separation. The combined effect of these variables is complex and the flow visualisation shows that the multiphase fluid mechanics that occur at the hydrophilic/hydrophobic branch is also complex and, at this stage, beyond accurate simulation. We have, however, developed a simple hydraulic model that goes some way to explaining the results and the development of this model is fully described below.

The flow situation is shown schematically in Fig. 5a and the mathematical model for pressure balance-driven separation is governed by eqn (2)–(4), *i.e.* the total mass conservation, the mass conservation of the water fraction and the pressure balance between mainstream and sidestream outlet. Fig. 5a depicts Δp_M and Δp_S as the pressure differences between point 1 and atmospheric pressure p_0 at the downstream ends of both the main- and sidestreams, respectively.

Total mass conservation:

$$Q_{in} = Q_M + Q_S \quad (2)$$

Aqueous mass conservation:

$$Q_{in}\alpha_{in} = Q_M\alpha_M + Q_S\alpha_S \quad (3)$$

Pressure balance of outlets:

$$\Delta p_M = \Delta p_S \quad (4)$$

Calculating the precise pressure drops Δp_M and Δp_S for multiphase slug flow is still an unresolved issue and certain simplifications are inevitable. For instance, Kashid and Agar[20] reported two approaches. One is derived from gas–liquid slug flow and takes account of the wall-film and length of the slugs. The second approach (chosen in this study) is given by eqn (5)

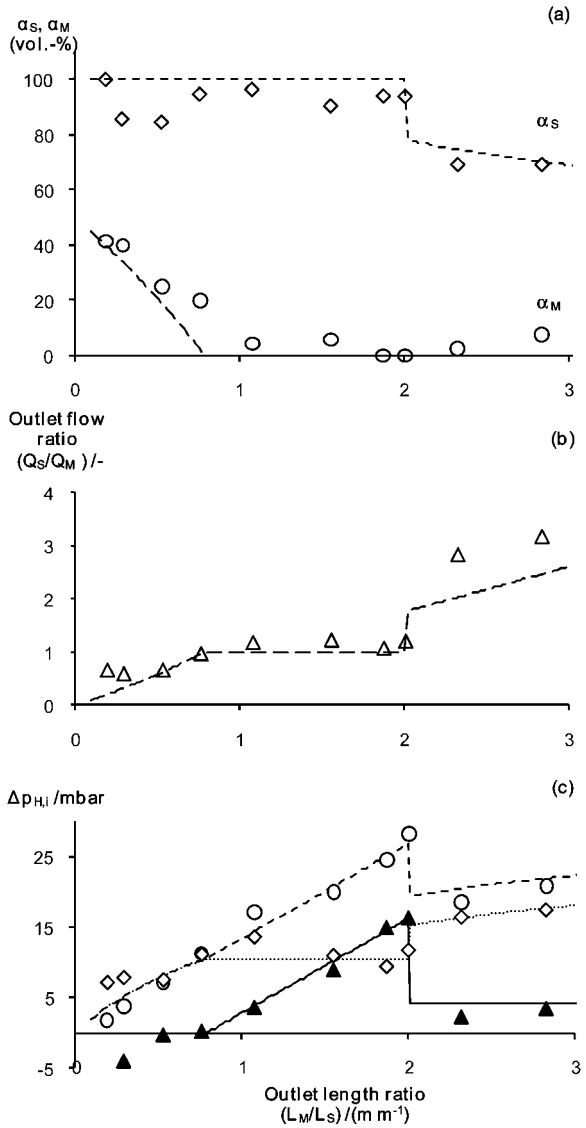

Fig. 4 Effect of L_M/L_S ratio for kerosene–water slugs separation on: (a) volumetric fraction of water in mainstream, α_M, and sidestream, α_S; (b) ratio of volumetric flow rates for the sidestream and mainstream, Q_S/Q_M; (c) frictional mainstream pressure drop (○), frictional sidestream pressure drop (◇), and difference in frictional pressure drop (▲). Dots in (a) to (c) represent average experimental measurement values, whilst lines present values predicted by the pressure balance model fully described in section 4 below (with a best-fitted value of $L_{Mc}/L_{Sc} = 2.0$ assumed in the model).

and includes two basic contributions. A Hagen–Poiseuille relation given by eqn (1) is assumed to account for frictional pressure drop, although wall-film and slug length are neglected, as well as the absence of laminar velocity profiles in the slug flow vortex pattern. The second term (which makes eqn (5) to differ from eqn (1) above) represents the Laplace pressure present in slugs, which is necessary to take into consideration when performing a pressure balance downstream point 1 (*i.e.* point of flow separation) because of the flow inversion at the hydrophilic sidestream capillary. Generating this excess pressure causes an additional pressure drop during the formation of organic-in-water slugs.

$$\Delta p_i = k_i'[\mu_o(1-\alpha_i) + \mu_w\alpha_i]Q_i + \frac{4\gamma\cos(\theta)}{d_i} \quad (5)$$

Hydrostatic and dynamic pressure drops are neglected and steady-state flow is assumed.

• Eqn (2)–(4) give three equations with four unknowns, namely Q_M, Q_S, α_M and α_S and in order to solve the equations certain boundary condition values were assumed for different regions of L_M/L_S. For very small values of L_M/L_S, no flow occurs through the sidestream, therefore Q_S/Q_M was set to zero, from which the composition in the mainstream, α_M, would equal the input value, *i.e.* $\alpha_M = \alpha_{in} = 0.5$.

• With an increase in L_M/L_S, and because of the hydrophilic nature of the sidestream needle, we assumed that only the aqueous phase flows through the sidestream, *i.e.* $\alpha_s = 1$, until L_M/L_S reaches the value of geometric parameter A that defines the "equilibrium set-point". The equation for parameter A is presented in Fig. 5b and had a calculated value for our system equal to 0.80. This situation is shown schematically in scenario I in Fig. 5b.

• In order for the organic phase to flow down the sidestream channel, the pressure difference between the two streams at the junction should exceed a certain value, inducing the flow inversion and enabling the flow of organic drops through the aqueous sidestream. This is expected to be directly controlled by the Laplace pressure of kerosene-in-water drops. Therefore, in practice, the $\alpha_S = 1$ assumption considered in scenario I is extended to a value of L_M/L_S above A such that the pressure balance and Laplace pressure equal and exceed the value calculated using eqn (5) for the sidestream. This point is represented by a critical ratio L_{Mc}/L_{Sc} shown schematically in Fig. 5c and should equalise to the sum $A + B$, where B is a parameter obtained during the mathematical manipulation of the pressure and mass balance equations and described in Fig. 5b (and equal to 0.31 in our system). The interval of L_M/L_S from A to $A + B$ represents the perfect separation scenario (scenario II in Fig. 5b).

• For values of $L_M/L_S > L_{Mc}/L_{Sc}$ (*i.e.* $A + B = 1.11$) the pressure in the separation junction point p_1 exceeds the selective "pressure barrier" to the organic phase (given by the Laplace pressure), therefore the organic phase can flow through the sidestream as shown schematically in scenario III of Fig. 5b. It is then assumed that all the aqueous phase is "captured" by the sidestream and therefore the volumetric water composition in the mainstream, α_m, approaches zero. This is a gross assumption that becomes more accurate as $L_M/L_S \gg 1$.

By following the above set of very simplistic assumptions, it is then possible to solve mathematically the mass and pressure balance equations for each region systems and the expected results are schematically represented in Fig. 5c. The figure illustrates how α_S, the volume fraction of aqueous in the sidestream, α_M, the volume fraction of aqueous in the mainstream and Q_S/Q_M, the volumetric ratios of flow rates, vary with the L_M/L_S ratio The model indicates that for L_M/L_S in the window from A to L_{Mc}/L_{Sc} a very efficient separation is achieved, whereas operation at a L_M/L_S value outside this region will result in one of the streams becoming contaminated with either the organic or aqueous phase.

4.2 Experimental model validation

The pressure balance model described in section 4.1 above was capable of predicting the experimental data reasonably well as

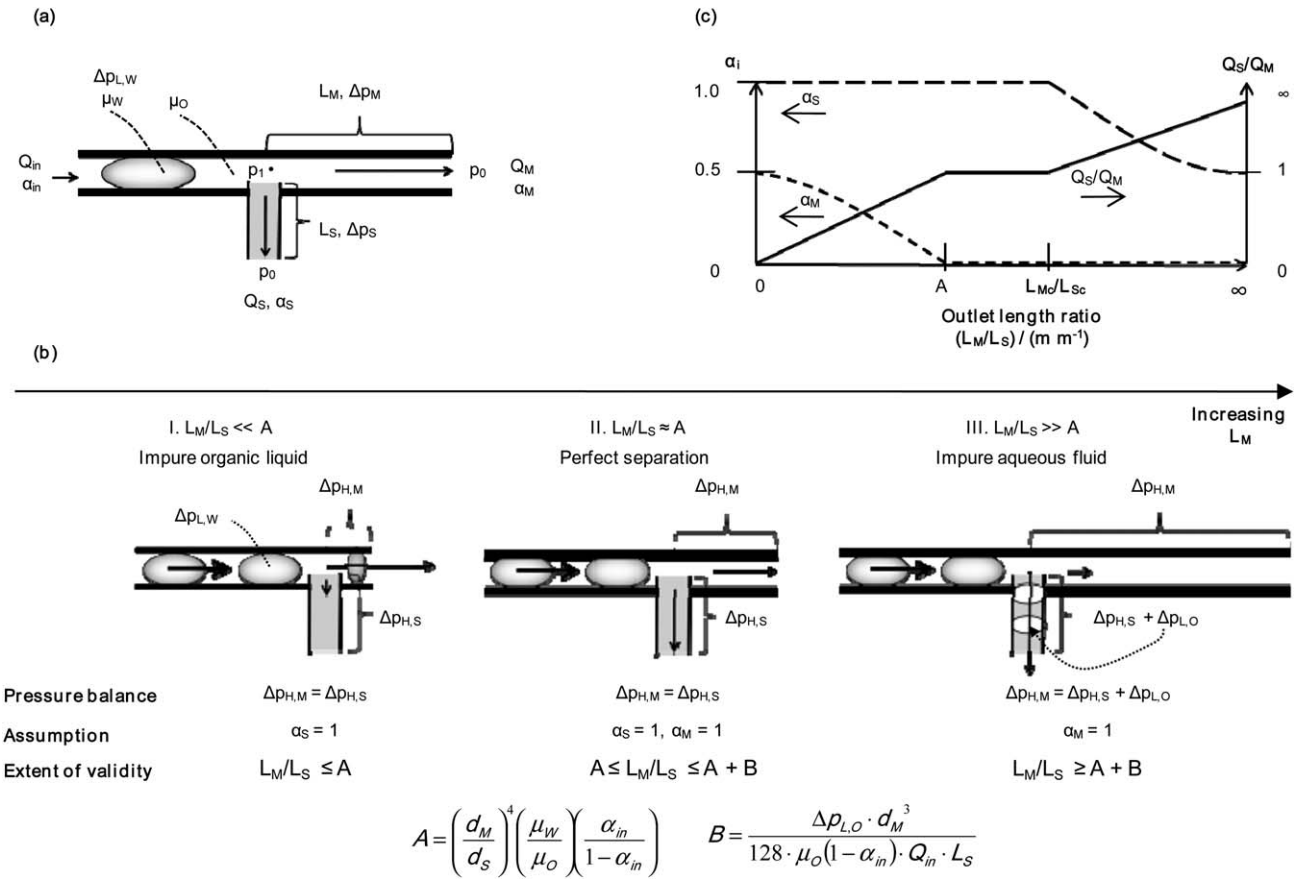

$$A = \left(\frac{d_M}{d_S}\right)^4 \left(\frac{\mu_W}{\mu_O}\right)\left(\frac{\alpha_{in}}{1-\alpha_{in}}\right) \qquad B = \frac{\Delta p_{L,O} \cdot d_M^{\,3}}{128 \cdot \mu_O (1-\alpha_{in}) \cdot Q_{in} \cdot L_S}$$

Fig. 5 Description of pressure balance model developed. (a) Important variables considered in the model. (b) Set of assumptions and equations considered for arbitrary L_M/L_S, Q_{in}, α_{in}, d_M, d_S, μ_O, μ_W. (c) Solution of pressure balance model equations for estimating the volumetric fraction of aqueous phase in hydrophilic sidestream, α_S, and hydrophobic mainsteam, α_M, and ratio of volumetric flow rates in sidestream and mainstream, Q_S/Q_M, as a function of effective length ratio L_M/L_S for kerosene–water separation in the MCF capillary ($\alpha_{in} = 0.5$).

shown in Fig. 4 above (model predictions were represented by lines). The model provided a good estimate of water composition, flow rate and pressure drop with increasing L_M/L_S ratio for both the main- and sidestreams, however, two minor modifications were required in the model in order to attain such good degree of matching. These consisted in best-fitting the two limits of transition of separation regime II, because the values experimentally obtained for parameters A and B significantly deviated from those predicted by our equations.

When modelling the pressure balance, errors in calculating the Laplace pressure in organic slugs can arise due to uncertainties in the exact surface tension and contact angle values. The critical length ratio L_{Mc}/L_{Sc} is governed by the Laplace pressure and this ratio was therefore adjusted to best-fit the experimental results giving a value of $L_{Mc}/L_{Sc} = 2.0$. This means in practice that regime II in Fig. 5b has extended beyond its predictions (*i.e.* $L_{Mc}/L_{Sc} > A + B$) presumably because of a pressure drop contribution not considered in one of the streams. The transition from regime II to regime III is dictated by the flow inversion through the sidestream, *i.e.* the point at which oil starts flowing through the aqueous phase therefore overtaking the Laplace pressure resistance. Once this happens, the pressure drop, stream composition and flow ratios are dictated by regime III, which explains the deviations from the plot in Fig. 5c and the step change in the modelled and experimental data shown in Fig. 4. From that, it could be concluded that a value of L_M/L_S of ~1 to 2 gives a useful window for operation of the separation process where separation performance is essentially constant and optimal.

A unique aspect of this pressure balance model is that it provides a good prediction of the pressure differences between the two streams, and here too a good fit was observed between the model and the experimental data, as shown in Fig. 4c. Inevitably, because of the simplifying assumptions that have been made in this model, there is some degree of deviation in the fit.

5. Discussion and conclusions

This paper has shown that it is possible to separate aqueous slugs dispersed in a continuous organic phase within an extruded plastic microcapillary. The process requires careful control of material properties, by choosing a hydrophobic surface for the purification of the organic phase and a hydrophilic surface for the purification of the aqueous phase, whilst balancing the downstream pressure differences between the two outlet streams. The process was found to be very sensitive to the viscosity ratio of the working fluids. The water–mineral oil system exhibited a substantial viscosity difference and the separation efficiencies

observed were very modest. The pressure balance model developed here demonstrates the importance of the Laplace pressure and highlights the need for pressure balancing between the side- and mainstreams for an efficient separation. An intrinsic feature of this model is the preferential flow of the aqueous phase through the metallic capillary and the organic phase through the plastic microcapillary.

The good agreement between the pressure balance model and experimental measurements for kerosene–water system is, however, based on a fixed value of the flow rate, composition ratio and for one microcapillary diameter, so that at this stage we are unable to say whether the model will be equally good for higher throughputs, entailing either increasing capillary diameter or a greater number of capillaries. Nevertheless, the observations and results show that if an immiscible slug flow can be generated within a plastic, hydrophobic microcapillary, using the techniques described, an effective phase separation can be achieved by simply piercing the wall of the downstream plastic capillary with a hydrophilic metal sidestream needle.

The efficiency of the aqueous–organic phase separation is influenced by a number of geometrical and rheological parameters, it is therefore difficult at the moment to extrapolate the model *a priori* to other immiscible systems. However, this technique has shown to be very simple but robust with appropriate microfluidic devices, and engineering the system could be developed into a viable commercial extruded, microfluidic separator. The pressure balance model developed is primarily sensitive to the surface tension of the immiscible system and the internal diameter of the hydrophilic sidestream, since these two parameters govern the Laplace pressure responsible for the selective distribution of the two phases between the two outlets and define the window of L_M/L_S values necessary to attain perfect separations. Provided an aqueous-in-organic continuous slug flow can be generated in the capillary, the pressure balance model offers an opportunity to fine tune the separation conditions systematically for the system under consideration. From both the experimental data and modelling presented in this paper it is now possible to design a microfluidic flow separator that can efficiently separate a hydrophobic/hydrophilic micro-slug flow. This represents a clear advantage over the more or less empirical design of such wettability discrimination liquid–liquid separators in the past.

Nomenclature

d	internal diameter, m
L	length of outlet channel or capillary, m
p	pressure, bar
Q	flow rate, $m^3\ s^{-1}$
Greek symbols	
α	volumetric water fraction, dimensionless
Δp	hydraulic pressure drop, bar
Δp_H	frictional pressure drop, bar
Δp_L	Laplace pressure drop, bar
Φ	angle of sidestream needle penetration, degrees
γ	surface tension, $N\ m^{-1}$
μ	viscosity, $N\ s\ m^{-2}$
θ	contact angle, degrees
ρ	density, $kg\ m^{-3}$
ξ	degree of needle penetration in the capillary, dimensionless
Subscripts	
c	critical
i	outlet channel *i*
in	inlet
M	mainstream
O	atmospheric
S	sidestream
W	water

References

1 T. Frising, C. Noik and C. Dalmazzone, *J. Dispersion Sci. Technol.*, 2006, **27**(7), 1035–1057.
2 D. A. Colman and M. T. Thew, *Chem. Eng. Res. Des.*, 1983, **61**(a), 233–240.
3 S. Schütz, G. Gorbach and M. Piesche, *Chem. Eng. Sci.*, 2009, **64**(18), 3935–3952.
4 P. Bley; W. Ehrfeld; G. Eisenbeiss, *International Patent*, 3877892, USA, 1975.
5 S. Ookawara, T. Ishikawa and K. Ogawa, *Chem. Eng. Technol.*, 2007, **30**(3), 316–321.
6 J. G. Kralj, H. R. Sahoo and K. F. Jensen, *Lab Chip*, 2007, **7**(2), 256–263.
7 H. Hartig; U. Kamecke, *International Patent*, WO 2005/028066 A1, Germany, 2005.
8 O. K. Castell, C. J. Allender and D. A. Barrow, *Lab Chip*, 2009, **9**, 388–396.
9 D. E. Angelescu, B. Mercier, D. Siess and R. Schroeder, *Anal. Chem.*, 2010, **82**(6), 2412–2420.
10 A. Aota, K. Mawatari, S. Takahashi, T. Matsumoto, K. Kanda, R. Anraku, A. Hibara, M. Tokeshiand T. Kitamori, *Microchimica Acta,* Springer, Wien., 2009, pp. 249–255.
11 F. Maso; I. Toru; I. Yasuo; M. Keiji; M. Yoshiro, *International Patent*, 05049809 A, Japan, 1993.
12 S. Koichi; K. Nobuhiro; T. Hiroshige, *International Patent*, 2009074563 A, Japan, 2009.
13 J. R. Burns and C. Ramshaw, *Chem. Eng. Res. Des.*, 1999, **77**(3), 206–211.
14 K. F. Hoettges; D. Stevenson; K. P. Homewood; R. M. Gwilliam, *International Patent*, WO 03/082429 A2, 2003.
15 M. N. Kashid, Y. M. Harshe and D. W. Agar, *Ind. Eng. Chem. Res.*, 2007, **46**(25), 8420–8430.
16 M. Mendorf, H. Nachtrodt, A. Mescher, A. Ghaini and D. W. Agar, *Ind. Eng. Chem. Res.*, 2010, **49**(21), 10908–10916.
17 C. H. Hornung and M. R. Mackley, *Chem. Eng. Sci.*, 2009, **64**(17), 3889–3902.
18 B. Hallmark, C. Parmar, D. Walker, C. H. Hornung, M. R. Mackley and J. F. Davidson, *Chem. Eng. Sci.*, 2009, **64**(22), 4758–4764.
19 D. C. Vadillo, T. R. Tuladhar, A. C. Mulji and M. R. Mackley, *J. Rheol.*, 2010, **54**(4), 781–795.
20 M. N. Kashid and D. W. Agar, *Chem. Eng. J.*, 2007, **131**(1–3), 1–13.